# Two-stage locally linearized SQUID readout for frequency domain multiplexed calorimeter arrays

**Mikko Kiviranta, Leif Grönberg and Hannu Sipola.**
VTT, Tietotie 3, 02150 Espoo, Finland

E-mail: Mikko.Kiviranta@vtt.fi

**Abstract.** We have constructed a two-stage SQUID amplifier intended for multiplexed cryogenic detector arrays. The upper SQUID is a locally linearized 6 x 80 array showing 0.13 $\mu\Phi_0$ $Hz^{-1/2}$ flux noise at 4.2 K. The lower linearized 4 x 3 SQUID array has decoupled input and feedback coils and shows 0.28 $\mu\Phi_0$ $Hz^{-1/2}$ flux noise at 4.2 K. Design principles and measured performance are reviewed.

## 1. Introduction

The demand for highly linear SQUID amplifiers, needed in Time Domain (TD), Code domain (CD) and Frequency Domain (FD) multiplexers, has recently driven attempts to contain the whole negative feedback path within the cryogenic stage [1 - 6]. The resulting small feedback delay would imply a large signal bandwidth, which is a necessity in multiplexing schemes where information content of several detector signals must be packed into a single amplification chain. Purely SQUID-based local negative feedback was pioneered by Irwin and Huber [7].

The last cryogenic stage should deliver the signal power which is by factor $D_X{}^2$ larger than the noise floor of the first room-temperature amplifier (LNA), where $D_X$ is the desired amplitude dynamic range at the linearity level prescription $X$ (see Appendix A). Due to the relatively large required signal power the early attempts [1-3] used a cryogenic transistor as the output stage. Even larger signal powers may be useful, as the result of the Appendix B suggests.

Recently Drung et. al. [6] have constructed narrowline SQUID arrays, intended for shield-less operation in the ambient magnetic field [8]. The technique also makes it possible to build very large SQUID arrays and still retain coherent operation of the constituent SQUIDs [9], because decohering localized flux traps cannot form in the narrow lines. Large enough output signal power can then be reached without cryogenic transistors.

Combining the narrowline- and local linearization approaches, we have constructed a two-stage SQUID amplifier whose both stages are linearized separately (Fig. 1). In this experiment the upper stage is a 6-parallel 80-series SQUID array and the lower stage is a 3-series 4-parallel array. This is continuation of our earlier work [9]. The choice of design parameters has been motivated by the Transition Edge Sensor (TES) -based X-ray calorimeters intended for the XEUS/IXO mission [10].

## 2. System level goals

The dimensioning of the amplifier chain is constrained by three goals. First, sufficient power gain is needed to raise the signal power from the noise floor at the TES output, order-of $10^{-24}$ W/Hz, to the roughly $10^{-21}$ W/Hz noise floor of the LNA. Depending on the achievable power gain per stage, this goal requires two or more cascaded amplification stages. Second, the power delivering capability of each stage must be at least $D_X{}^2$ times higher than noise floor of the subsequent stage. Third, sufficiently low distortion needs to be achieved over the $D_X$. To alleviate reaching the goals, noise matching and power matching between the stages should be enforced.

### *2.1 Power gain*

The figure-of-merit describing the gain of a SQUID is the ratio of available output power to the energy stored in the input coil $dP_O / dE_I$. When the SQUID input inductance $L_I$ is driven from a resistive generator[1] $R_G$ whose available power is $P_G = \frac{1}{2} R_G I_G^2$, a -3dB cutoff $\omega_C = R_G / L_I$ is implied.

[1] A series capacitor can be used to tune out the $L_I$, in which case the bandwidth $\omega_C$ is centered around the tuning frequency rather than dc.

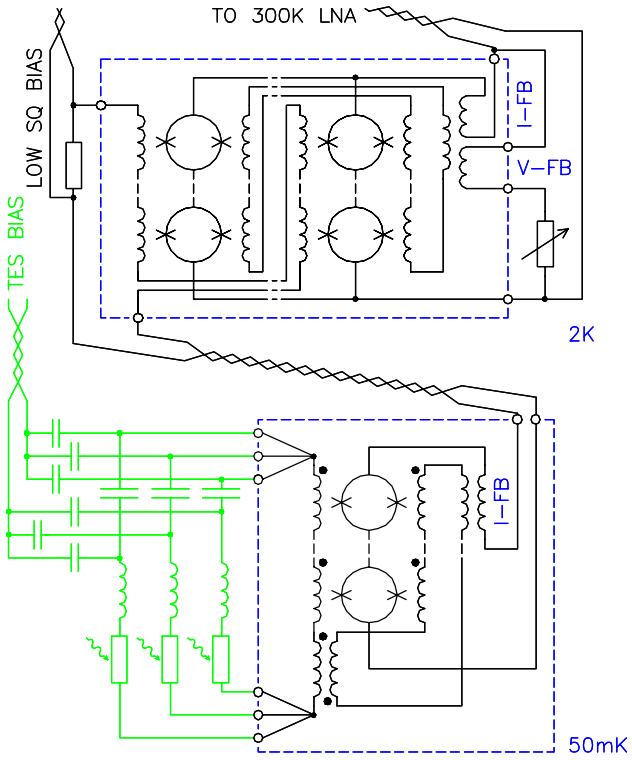


Figure 1: Simplified schematic of the readout circuitry.

The stored energy is $E_I = P_G / \omega_C$ when operating at frequency $\omega = \omega_C$ and approaches twice the value when $\omega << \omega_C$. One can write

$$\frac{dP_O}{dP_G} = \frac{\frac{1}{2} R_D \left(\partial I / \partial \Phi \cdot M\, I_G\right)^2}{\frac{1}{2} \omega_C L_I I_G^2}, \qquad (1)$$

where $R_D$ is the dynamic resistance of the SQUID output, $M$ is the mutual inductance of the input and $\partial I / \partial \Phi$ is the current gain of the SQUID. For the dc SQUID at noise optimum [11] $\beta_C = 0.7$, $\beta_L = 1$ this simplifies to

$$\frac{dP_O}{dP_G} = \frac{k_C^2 \zeta_D}{2\omega_C \sqrt{L_{SQ} C_J}} \qquad (2)$$

in the $\omega << \omega_C$ operating region. Here $k_C$ is the magnetic coupling constant of the input coil and $\zeta_D$ is the ratio of the dynamic output resistance to the shunt resistance. The term $(L_{SQ}\, C_J)^{-1/2}$ involving the SQUID loop inductance and Josephson junction capacitance coincides with the plasma frequency $\omega_P$ [12] of the tunneling barrier. Within a given material technology, increase of the critical current density $J_C$ of the barrier raises the $\omega_P$. The recipe to improve $dP_O / dE_I$ is therefore to boost the $J_C$ until the associated decrease of $L_{SQ}$ causes the coupling $k_C$ to deteriorate too much. The quest for a large $dP_O / dE_I$ drives the design of individual SQUID cells, which are used as building blocks for the arrays. Because $\partial V / \partial \Phi$ of a SQUID can be shown to be proportional to $\omega_P$, a large $\omega_P$ also implies a low noise temperature [13]. Those SQUID amplifier parameters which scale directly proportional to $\omega_P$ are not affected by array dimensions when constructing an array.

### *2.2 Maximum output power and heat dissipation*

The second goal is to provide output signal power delivering capacity $P_{O,MAX}$ in the final stage such that, after losses and added Johnson noise of the cabling, the signal that reaches the LNA is by the factor $D_X^{\,2}$ above its noise floor. In lower stages the $P_{O,MAX}$ must reach that of the final stage divided by the cascaded power gain (Eq. 1). The sufficient $P_{O,MAX}$ is obtained by choosing the total number $k \times m$ of SQUID cells in a $k$-parallel $m$-series array.

Dc SQUIDs resemble class-A transistor amplifiers in the sense that their static power dissipation equals a constant factor times $P_{O,MAX}$. Because each microwatt dissipated at a low temperature $T_0$ is worth more heat at a higher temperature $T_1$ at least by the Carnot efficiency[2], the total system dissipation at 300K is minimized when each amplifier stage is moved to as high temperature as the available refrigerator temperatures, cabling considerations and SQUID noise allow. The SQUID noise performance tends not to improve below approximately 0.3 K bath temperature [14], which suggest that a sole step-up transformer might be adequate at the 50 mK base temperature, the first SQUID residing at T ≥ 0.3 K.

### *2.3 Linearization*

The local negative feedback [4] can be arranged by sampling the output current (I-FB) or output voltage (V-FB) of the SQUID. The negative I-FB linearizes the current response, decreases the current gain $\partial I / \partial \Phi$ and increases $R_D$ by the factor $\mathcal{L}_I + 1$ where $\mathcal{L}_I$ is the current sampling loop gain. The voltage response remains intact. Similarly, the negative V-FB linearizes voltage response, decreases voltage gain $\partial V / \partial \Phi$ and suppresses $R_D$ proportional to $\mathcal{L}_V$, the V-FB loop gain, but keeps the current response intact. In the SQUID input side there are two choices as well: feedback signal can be injected in a shunt or series configuration and this choice affects the input impedance, analogously. Contrary to our claim in [9], the reduction of $\partial I / \partial \Phi$ or $\partial V / \partial \Phi$ does not necessarily lead to straightforward loss of $dP_O / dE_I$, because feedback also screens $L_I$ (Eq. 1),

[2] In practice by the real refrigerator efficiency which is much worse.

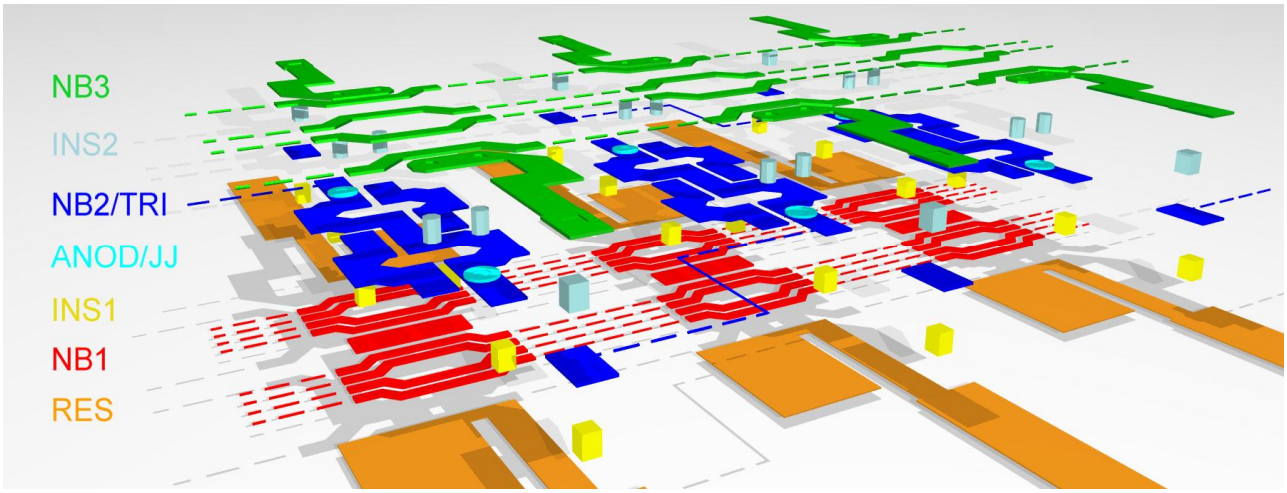


Figure 2: The 3D exploded view of the SQUID cell design and the fabrication stack.

provided that there is magnetic coupling between the feedback and input coils.

*2.4 Interstage matching*

Interstage matching involves both power matching, i.e. arranging impedance levels such that maximum signal power transfer occurs, and noise matching, i.e. guaranteeing that the combined back-action noise and direct noise has the lowest possible joint impact.

The direct way to affect output impedance of a SQUID array is to vary its aspect ratio $m : k$. The input impedance depends on the number of turns $n$ in the input coil, but not on the aspect ratio because the input coils of an array must in practice be coupled in series, to avoid superconducting loops.

Although feedback influences locally the output impedance of a SQUID stage, the full-swing power delivering capability is not affected. It is optimal to reach maximum current swing and maximum voltage swing simultaneously, but their turnpoint-to-turnpoint (TP-TP) values cannot be affected by feedback.

The noise matching impedance or noise temperature at the input of the SQUID, like any linear amplifier, does not (within certain realistic assumptions) change by introducing feedback [15]. Therefore feedback can be used to shift the power match and noise match to the same impedance.

We have chosen to use simultaneous I-FB and V-FB in the upper stage, which drives the LNA and where the largest swings are required. Then the $R_D$ does not change from its non-feedback value. The advantages are that (i) the full-swing power match equals finite-swing power match; and that (ii) the SQUID-to-LNA cable is match-terminated also at its low end, which prevents formation of standing noise waves due to the LNA back-action.

## 3. SQUID design

*3.1 The basic SQUID cell*

The basic SQUID element is a gradiometric 40 pH loop, equipped with 2.5 μm diameter Josephson junctions. Junctions are defined by anodization from a Nb/Al-AlOx/Nb trilayer with the nominal 500 A/cm$^2$ critical current density. A superconducting Nb wiring layer is available both under the trilayer and on top of it. Junctions are shunted with nominally 4.5 Ω Pd resistors which are located in the same plane as the lowermost wiring layer for the lowest Kapitza resistance to the substrate. All the superconducting lines are at most 6 μm wide in order to avoid flux traps [8] even when the device is cooled in earth's magnetic field. Using contact lithography we were able to align a 2-turn input coil underneath the 6 μm wide SQUID loop and form a 1-turn feedback coil on top of it. PECVD deposited $SiO_2$ is used as the insulation layers. The lower $SiO_2$ is grown at 300 C and CMP planarized, in order to provide a smooth surface for the trilayer deposition. The higher $SiO_2$ is deposited at 180 C. All contact windows are plasma etched, and an extra protective layer is formed on top of the trilayer to avoid plasma induced damage during the via etch. The process layers are shown in Fig. 2.

The SQUID cell design is cascadable into large format arrays. The bias current flows through the diagonally opposed corners of the gradiometric loop, effecting a symmetric bias current path. All the local feedback is hence achieved via the feedback coil

*3.2 Upper SQUID*

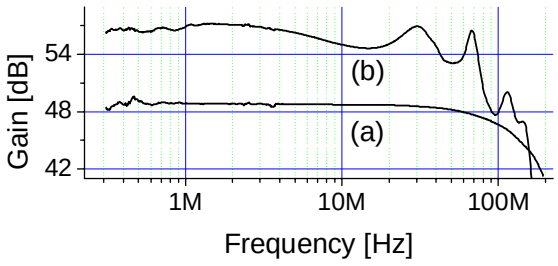


Figure 3: (a) Frequency response of the plain LNA. (b) Frequency response of the LNA + dipstick combination (gain baseline shifted by ~ 10 dB for a clearer plot).

The upper device is a 80-series 6-parallel array of the SQUID cells. The array output current flows through an intermediate transformer with 85 $\mu A/\Phi_0$ coupling to create current-sampling feedback (I-FB) [4]. A flux setpoint coil and a voltage-sampling feedback coil with 42 $\mu A/\Phi_0$ coupling are additionally integrated in the transformer, whose washer-like construction *does* contain wider than 6 μm superconducting structures.

A low-capacitance GaAs MESFET is used as an adjustable resistor controlling the V-FB loop gain (Fig. 1). Previously we used an ADG804 multiplexer to select the feedback resistor, whose large parasitic capacitance tuned the feedback coil and caused plateaus in the SQUID characteristics [9].

*3.3 Lower SQUID*

The total number of SQUIDs in the lower array is limited to 12, by the desire to keep the power dissipation low and to keep the input inductance below 4 nH. Similar to our previous design [16] there are multiple input pad pairs which lead to the low inductance summing point.

The aspect ratio of the array was chosen for a sufficiently high linearized $\partial I / \partial \Phi$ to obtain 1:1 flux ratio between the upper and lower SQUID, and simultaneously a sufficiently high L/R cutoff frequency. The cutoff frequency is due to the dynamic resistance of the lower array and combined inductance of the interstage wiring and upper SQUID input.

In the SQUID version used in this experiment, there is a circuit to decouple the feedback coil from the input coil. Coupling constants of three-coil systems in general are constrained by the Tokad-Reed [17] criterion

$$k_1^2 + k_2^2 + k_3^2 - 2k_1k_2k_3 \le 1 \qquad (3)$$

A commonly used decoupling arrangement is a

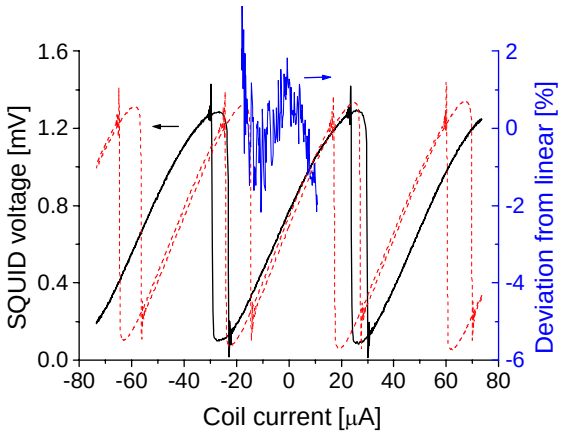


Figure 4: Output voltage of the two-SQUID cascade as a function of the input coil current (solid line) and flux response of the upper SQUID alone at the used V-FB setting (dashed line). Also depicted is the non-linearity of the two-SQUID response.

gradiometric SQUID loop where feedback coil couples to one half and input coil to the second half of the gradiometer, which corresponds to the case $k_1$ = 0.7, $k_2$ = 0.7 and $k_3$ = 0. We wished to improve the input coil coupling at the cost of feedback coupling, so that instead of the half-half gradiometric coupling there is a compensating transformer at the end of each 3-SQUID chain. Neglecting parasitics, our arrangement would correspond to the case $k_1$ = 0.86, $k_2$ = 0.5 and $k_3$ = 0.

## 4. Low noise amplifier

The room-temperature Low Noise Amplifier (LNA) is a dc-coupled differential pair of BFP650 silicon-germanium bipolar transistors, whose very low voltage noise [18] is advantageous in this application. The LNA utilizes active termination [19] to obtain an effective low-temperature 60 Ω termination for the twisted pairs which connect the LNA to the cryogenic stage. Active termination is a standard technique which has found earlier use also in SQUID readouts [18, 20, 21]. The bandwidth of the plain LNA is 120 MHz and looping back a test signal through the dipstick wiring indicates 40 MHz useable bandwidth (Fig. 3). The dynamic resistance of the upper SQUID has been dimensioned to terminate the cold side of the twisted pairs, to prevent rotation of the source impedance in the Smith chart as seen by the LNA. The varying source impedance would otherwise make the noise mismatch frequency dependent. The measured white noise performance of the LNA with $u_N$ = 0.38 nV/Hz$^{1/2}$ and $i_N$ = 7.4 pA/Hz$^{1/2}$ is worse than expected, and a construction of an improved LNA is underway. Noise measurements were

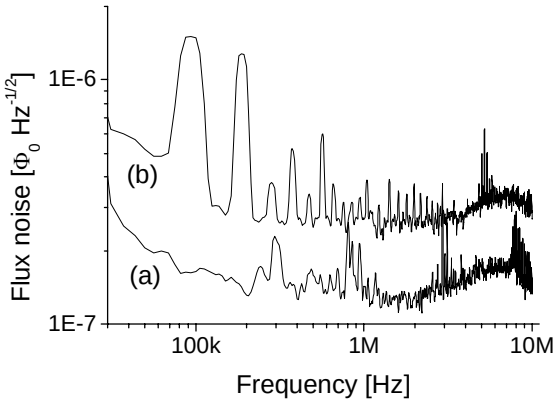


Figure 5: (a) Flux noise of the upper SQUID, when operated in the I-FB linearized slope, V-FB is inactive and lower SQUID is not connected. (b) Flux noise of the lower SQUID, measured through the upper SQUID.

performed using 13 Ω, 50 Ω and 200 Ω cold resistors at 4.2 K as loads, switched with a cryogenic mechanical relay[3].

## 5. Experiments

### *5.1 Noise, bandwidth and linearity*

The experiments were performed by immersing the SQUIDs into liquid He in a dipstick. The dipstick is wired using Lake Shore DT-32 twisted pairs, and Samtec FTSH-DH 1.27 mm pitch headers are used as connectors.

First the upper SQUID, i.e. the 6 x 80 array, was measured separately without the lower SQUID attached. Only the hard-wired I-FB linearization was active during these measurements. The resulting flux response, flux noise level and frequency response are shown as the first set of curves in Figs. 4, 5 and 6.

Next, the lower SQUID was coupled to the amplification chain. The V-FB loop gain of the upper SQUID was raised slightly above zero, to the level that the full flux response of the lower SQUID can be recorded without inducing flux jumps in the upper SQUID. The loop gains were approximately $\mathcal{L}_I = 0.8$, $\mathcal{L}_V = 0.3$ . The obtained flux response, flux noise spectrum and frequency response are shown as the second set of curves in Figs 4, 5 and 6. The realized mutual inductance of the input coil is $M^{-1} = 38\ \mu A/\Phi_0$ for both the upper and the lower SQUID.

Next, the two-stage cascade was excited by a 1 MHz sinusoid at different peak-to-peak amplitudes.

[3] Omron G6JU, whose latching capability and the high RRR of the coil wiring imply low heat generation even at sub-kelvin temperatures during the switching events.

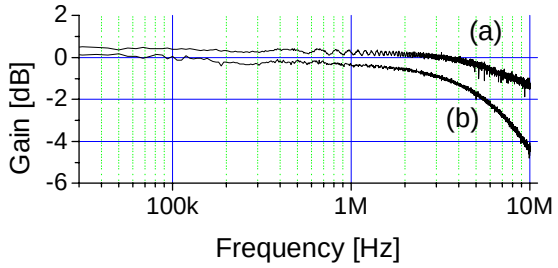


Figure 6: (a) Frequency response of the upper SQUID, when the operated in the I-FB linearized slope, V-FB is inactive and lower SQUID is not connected. (b) Frequency response of the two-SQUID cascade. A frequency chirp with 0.1 $\Phi_{0p\text{-}p}$ amplitude was used as the excitation.

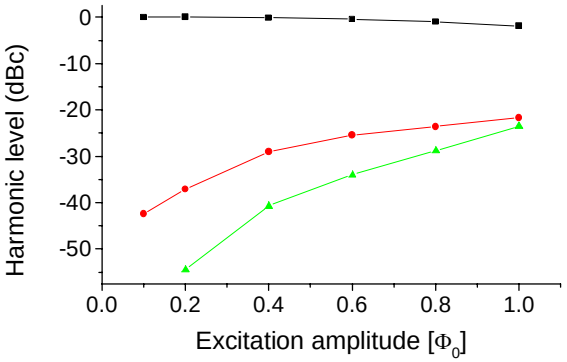


Figure 7: Suppression of the fundamental frequency (square), the 2nd harmonic level (ball) and the 3rd harmonic level (triangle) as a function of the peak-to-peak amplitude of a 1 MHz flux excitation.

Amplitude suppression of the fundamental frequency, as well as 2nd and 3rd harmonic amplitudes relative to the fundamental are depicted in Fig. 7.

Finally, input inductance of the lower SQUID was studied by observing the R/L cutoff when an input is shorted by a resistive bond wire. $L_I$ = 3.4 nH at the summing point was measured, plus 2 – 4 nH due to Josephson-blocking filters and wiring to each bonding pad pair.

### *5.2 Temperature dependence of the SQUID gain*

The major multiplexing methods TDM, FDM and CDM pursued today are based on amplitude modulating the fingerprint functions [22] by the TES signal, and therefore depend on the gain accuracy of the amplification path. Although one multiplexing channel can be reserved for gain calibration, the gain stabilities of the LNA and SQUIDs remain an issue. An additional concern is the stability of the active termination provided by

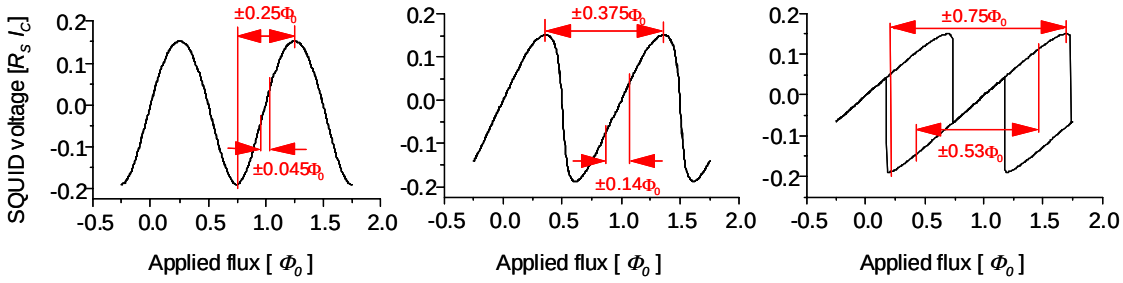


Figure 8: Simulated flux characteristics of a match-biased dc SQUID with $\beta_C = 0.7$ $\beta_L = 1$. The full dynamic ranges and the 1% total harmonic distortion limited dynamic ranges are indicated when current sampling loop gains are $\angle_I = 0$, 0.5 and 2.

the LNA, as the drift of its value would lead not only to gain variance but also to frequency dependence of the 4K-to-300K transmission line.

To address the question of the SQUID gain, we biased the 6x80 array at a typical operating setpoint, and measured the gain at various temperatures from 0.5 K to 2.5 K in a Heliox $^3$He sorption cooler. Such effects as the flux setpoint drift and shunt resistor variance as a function of temperature were noted to be negligible, and the observed gain dependence is consistent with Ambegaokar-Baratoff variation [23] of the critical current alone, following temperature dependence of the superconducting gap [24].

*5.3 Discussion*

Experiments showed that our shunt resistor values were approximately one-half of the design values. The ensuing suppression of $dP_O / dE_I$ rendered the 4x50 array also present on the mask set suboptimal with our LNA, and forced us to use the larger 6x80 array instead. Another outcome was the low L/R cutoff frequency (Fig. 6 (b) ) between the lower and upper SQUID stage. The origin of the low $R_S$ value was deduced to be the PECVD $SiO_2$ deposition of the INS1 layer (Fig. 2) which was grown at 300 C instead of our standard 180 C. The consequent annealing of the buried Pd layer resulted in approximately doubling of the 300K/4.2K resistance ratio w.r.t. our unannealed Pd films.

We were forced to use predominantly I-FB and very light V-FB in the upper SQUID, in an attempt to enhance the deteriorated $R_D$ of the upper SQUID to a closer match with the LNA and cabling. The obtainable $\angle_I$ was limited, too, because of the stronger-than-designed suppression of the $\partial I / \partial \Phi$ by the 60 Ω LNA loading.

The obtained critical current density 400 A/cm$^2$ was slightly lower than the design value. We attribute this to the new plasma damage protecting Al film on top of the trilayer, which has been absent in our previous designs.

Between the lower and upper SQUIDs the small-signal R/L cutoff is defined by the feedback-enhanced $R_D$ as we claim in [9]. However, we have overlooked the fact that the I-FB loop gain begins to fall at frequencies above the *unenhanced* R/L corner, and hence the full-swing bandwidth of the system is determined by this.

The static power dissipation of $P_D$ = 0.5 nW per cell at the setpoint can be deduced from the measured IV characteristics.

Preliminary measurements at SRON [25] indicate significantly lower than $10^{-7}$ $\Phi_0$ Hz$^{-1/2}$ flux noise for the two-stage amplifier with the linearized response when temperature is below 0.3 K.

## 6. Conclusion

Even with imperfections discussed above, the present two stage amplifier provides very high performance. The lone upper stage provides $D = 10^7$ Hz at 4.2K with approximately 20 MHz -3dB bandwidth. The two-stage amplifier provides $D = 4.5\times10^6$ Hz, $D_{1\%} = 4.5\times10^5$ Hz and 7 MHz bandwidth. The obtained energy resolution is ε = 290 h at 4.2 K.

Although the devices contain wideline transformer structures in addition to the narrowline SQUID loops, the arrays are operable without superconducting shields, although the penalty in the performance has not been studied in detail.

Device performance is sufficient for using them in IXO-related FDM calorimeter experiments. Sub-kelvin measurements are underway.

## Acknowledgement

This work has been supported by the contract TRP5417 by the European Space Agency. We have gained from discussions with our consortium

partners from SRON and PTB Berlin and in particular from the brainstorming sessions with Jan van der Kuur.

## Appendix A: Dynamic range concepts

We take the 'full' dynamic range $D$ to mean the peak-to-peak flux amplitude between the turning points of the SQUID response, divided by the noise equivalent flux at the SQUID input, over unit bandwidth. Therefore its dimension is $\mathrm{Hz}^{1/2}$.

In practice, the tolerable maximum flux range is often less than the half-period of the SQUID response. One useful flux range prescription is to define the maximum allowed total harmonic distortion (THD) when a sinusoidal test signal is applied to the SQUID. We refer to such prescriptions by adding a relevant subscript $D_X$ to the symbol, eg. $D_{1\%}$ when THD must remain lower than 1%, i.e. 40 dB below the carrier.

To illustrate, we have simulated Josephson dynamics of a match-biased dc SQUID with $\beta_C$ = 0.7 and $\beta_L$ = 1 to obtain its flux response both without feedback and with negative feedback applied. The simulation was performed with the commercial APLAC circuit simulator, whose component library includes the Josephson junction. In Fig. 8 we have plotted the maximum sinusoidal flux deviation from the $\Phi_{set} = \Phi_0 / 4$ setpoint, which keeps the THD below 40 dBc, and the turnpoint-to-turnpoint (TP-TP) deviation.

By loop gain we mean the global loop gain, determined by the current or voltage modulation depth $\Delta I$ or $\Delta V$, rather than the local loop gain determined by the local slope $\partial I / \partial \Phi$ or $\partial V / \partial \Phi$. The global loop gain is less arbitrary, leads to worst-case linearity estimates for the full swing and gives a predictable estimate for the TP-TP flux range $\Delta\Phi_{TP-TP} = \pm\frac{1}{4}\Phi_0 \cdot (L + 1)$.

## Appendix B: Cryostat cabling as a communication resource

In absence of superconducting cables for the relevant temperature range, the Wiedemann-Franz law ties the thermal resistance $R_T$ for a cable leading from temperature $T_0$ to $T_1$ and its electrical resistance $R_E$ so that the heat leakage through the cable can be roughly written as

$$P_T = \frac{T_1 - T_0}{R_T} \approx \frac{T_1^2 L_W}{R_E \ln(T_1 / T_0)}. \quad (4)$$

$L_W$ is the Wiedemann-Franz constant and we assume $T_0 << T_1$. We denote the transmission line impedance of the cable as $Z_C$, and remark that it is difficult to make vastly different from the environmental impedance $\varepsilon_r^{-1/2} \times 377\ \Omega$. When warm end of the cable is terminated by a $Z_C$ -matched zero-noise LNA and cold end by a $Z_C$ -matched SQUID, the available power at the SQUID output which would correspond to the Johnson noise and losses due to $R_E$, is $P_{SQ,N} = 2k_B T_1 R_E / Z_C$. The maximum signal power $P_{O,MAX}$ the SQUID must deliver is $D^2$ times this, and we assume SQUID heat generation equals $P_{O,MAX}$. The combined thermal load due to SQUID dissipation and heat leakage of the cabling is minimized when

$$R_E = \frac{1}{D}\sqrt{\frac{T_1 L_W Z_C}{2k_B \ln(T_1 / T_0)}}. \quad (5)$$

For instance, taking $T_0$ = 4 K, $T_1$ = 300 K, $Z_C$ = 50 Ω, $D = 10^6$ Hz and $k_B = 1.38\times10^{-23}$ W/K we obtain the optimal cable resistance $R_E$ = 1.8 kΩ.

A more relevant optimization is finding the Shannon channel capacity of the cable, within a given combined power constraint $P_D$. An ideal terminated lossy transmission line does not have a theoretical high-frequency cutoff, needed for the Shannon calculation. The practical cutoff must be due to non-idealities, such as conductor roughness or excitation of transverse modes. If the cutoff frequency is taken to be where the skin effect kicks in and the cable loss becomes $f^{1/2}$ dependent, the Shannon channel capacity can be written as

$$C = \frac{R_E}{\mu_0 \ell}\log_2\left(1 + \frac{\mu_0 \ell D^2}{R_E}\right), \quad (6)$$

where $l$ is the cable length and $\mu_0$ is the vacuum permeability. Writing in the SQUID dissipation and heat leakage of the cable, one ends up with a non-linear optimization task, which tends to lead to even higher cable resistance optimum than the Eq. 5. We take these results as indications that it is fruitful to explore the regime where the SQUID power is large and the cable is very lossy.

## References

[1] Kiviranta M 2006 Use of SiGe bipolar transistors for cryogenic readout of SQUIDs *SuST* **19** 1297-1302 .

[2] Drung D et al 2007 Highly Sensitive and Easy-to-Use SQUID Sensors *IEEE Tran. Appl. Supercond.* **17** 699-704 .

[3] Mück M 2002 Increasing dynamic range of a SQUID amplifier by negative feedback *Physica C* **368** 141-5.

[4] Kiviranta M 2008 SQUID linearization by current-sampling feedback *SuST* **21** 045009 .

[5] Lanting T. M. et al 2009 Linearized superconducting interference device array for high bandwidth frequency-domain readout multiplexing *Rev. Sci. Instr*. **80** 094501 .
[6] Drung D et al 2009 Novel SQUID Sensors with High Linearity at High Frequencies *IEEE Tran. Appl. Supercond.* **19 772-7**.
[7] Irwin K D and Huber M E 2001 SQUID Operational Amplifier *IEEE Tran. Appl. Supercond.* **11** 1265-70.
[8] Stan G, Field S. B. and Martinis J. M. 2004 Critical Field for Complete Flux Expulsion in Narrow Superconducting Strips *PRL* **92** 097003 .
[9] Kiviranta M and Grönberg L 2009 Progress Towards Large Locally Linearized SQUID Arrays *AIP Conf. Proc* . **1185** 526-9.
[10] De Korte P et. al. 2008 EURECA – a European-Japanese microcalorimeter array *Proc. SPIE* **7011**, 701122
[11] Ryhänen T, Seppä H, Ilmoniemi R and Knuutila J 1989 SQUID Magnetometers for Low-Frequency Applications *J. Low Temp. Phys.* **76** 287-386.
[12] Solymar L 1972 *Superconductive Tunneling and Applications*, Chapman and Hall Ltd, London, 176.
[13] Hilbert C and Clarke J 1985 DC SQUIDs as Radiofrequency Amplifiers *J. Low Temp. Phys.* **61** 263-80.
[14] Wellstood F C 1988 *PhD Thesis* UC Berkeley.
[15] Haus H A and Adler R B 1959 *Circuit Theory of Linear Noisy Networks* John Wiley & Sons, Inc, New York.
[16] Kiviranta M et al 2004 Design and performance of multiloop and washer SQUIDs intended for sub-kelvin operation *SuST* **17** S285-9.
[17] Tokad Y and Reed M B 1960 Criteria and Tests for Realizability of the Inductance Matrix, *Tran. AIEEE Part I* **78** 924-6.
[18] Kiviranta M et al 2006 A post-SQUID amplifier aimed for multiplexed detector readouts *SuST* **19** S371-5.
[19] Percival W S 1939 An Electrically “Cold” Resistance *Wireless Engineer* **16** 237-40.
[20] Penny R D et al 1997 Wideband front end for high-frequency SQUID electronics *IEEE Tran. Appl. Supercond.* 7 2323-6.
[21] Drung D, Hinnrichs C and Barthelmess H-J 2006 Low-noise ultra-high speed dc SQUID readout electronics *SuST* **19** S235-41.
[22] Kiviranta M, Seppä H, van der Kuur J and de Korte P 2002 SQUID-based Readout Schemes for Microcalorimeter Arrays *AIP Conf. Proc* . **605** 295-300.
[23] Ambegaokar V and Baratoff A 1963 Tunneling between superconductors *PRL* **10** 486-9.
[24] Einzel D 2003 Interpolation of BCS Response Functions *J. Low Temp. Phys.* **130** 493-508.
[25] Lindeman M et al, unpublished.